ISSN 1061-3862, International Journal of Self-Propagating High-Temperature Synthesis, 2010, Vol. 19, No. 4, pp. 227–236. © Allerton Press, Inc., 2010.

SHS Reactions in Nanosized Multilayers: Analytical Model Versus Numerical One[1]

T. V. Zaporozhets[a], A. M. Gusak[a], and A. I. Ustinov[b]

[a]*Cherkasy National University, blvd. Shevchenko 81, Cherkasy, 18017 Ukraine*

[b]*Paton Institute of Electric Welding, National Academy of Sciences, Kiev, Ukraine*

e-mail: zaptet@ukr.net

Received August 2, 2010

Abstract—SHS reactions in solid nanosized multilayers yielding a single-phase product were modeled numerically and analytically. Scaling behavior of the product "burning velocity × multilayer period" was predicted. The effect of mean vacancy free pathlength and initial vacancy supersaturation on the SHS rate was investigated numerically. Within a wide range of process parameters, the front velocity appears to be inversely proportional to the square root of mean vacancy free pathlength.

Keywords: SHS, thin multilayer films, diffusion, modeling, non-equilibrium vacancies

DOI: 10.3103/S1061386210040011

1. INTRODUCTION

SHS technology, known since the 60s [1–5], came to our attention when we initiated the research project aiming at the development of a reliable process for diffusion welding of intermetallic multifoils [6, 7]. To control the main characteristics of SHS reactions (burning velocity and maximal front temperature), one has to take into account numerous factors, such as composition of multifoils, their overall thickness and period, structure of as-prepared multilayer (level of deviation from equilibrium, concentration of defects, pre-existing intermetallic layers), and ignition parameters (temperature and exposure). Mathematically, control of SHS reactions means the solution of inverse problem, i.e., finding out the magnitudes of above mentioned parameters that would provide required burning velocity and maximal temperature.

Moreover, mathematical modeling of SHS in multifoils looks more transparent and predictable in comparison with powder mixtures, since in this case one can use diffusion equations with known diffusion parameters (activation energy and pre-exponential factor), contrary to the case of powders when one has to use general equations with fitting coefficients for the reaction rate and ambiguous interpretation.

Generally, SHS reactions are being treated in nonstationary conditions since SHS systems normally have complex phase diagrams with numerous intermediate phases. These phases can grow either sequentially or simultaneously, so that SHS process must be described as a competition between exothermic and endothermic reactions with varying local temperatures. Varied temperature is accompanied by changes in the phase composition of products and formation of different heat sources. The process is strongly nonlinear, so that small changes may lead to bifurcation of regimes or full redetermination of phase evolution. All this makes mathematical modeling of SHS very difficult.

SHS in multilayers can be treated in the frame of a physical approach that represents chemical reaction as a sequence of diffusion-controlled phase transformations in the field of concentration gradient (which is nearly transversal to temperature gradient).

In many cases, SHS reaction yielding a single-phase product can propagate over multilayer in a steady mode. Such a situation was modeled for the case when the reaction was reduced to a continuous interdiffusion process and heating was distributed over the entire diffusion zone within the SHS flame [8]. The presence of pre-existing diffusion layer along the entire length of multilayer was taken into account. All non-equilibrium factors (finite relaxation rate of vacancies, as-prepared defect structure of multilayers) were neglected. In our opinion, such an approximation is insufficiently adequate. Indeed, the characteristic times of heating in the SHS front are typically very short—shorter than the characteristic vacancy relaxation times. Vacancy subsystem cannot keep up with the temperature change. It means that the actual values of vacancy concentration in any local region of SHS front do not correspond to the local temperature. Diffusivity is proportional to the actual vacancy concentration. So, we cannot use the temperature dependence of diffusivity taken from standard Arrhenius law for description of SHS.

[1] The text was submitted by the authors in English.

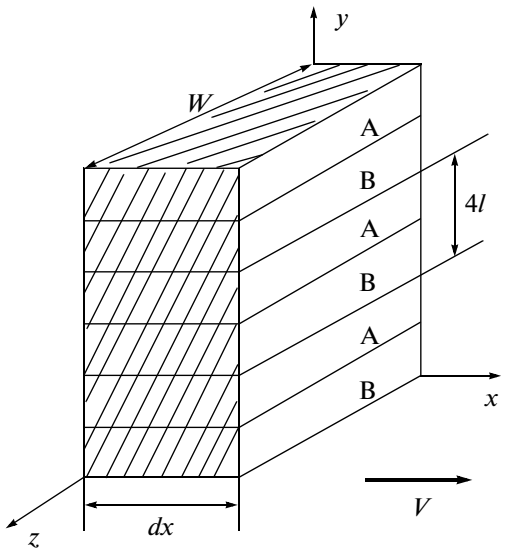

Fig. 1. Schematic of multilayer binary foil.

In this paper, we suggest a model of steady SHS process describing: (a) formation of single-phase product with a narrow homogeneity range when all heat is produced at the moving interphase boundaries; (b) deviation of local vacancy concentration (and corresponding diffusivities) from the local equilibrium values due to finite relaxation rate of vacancies; and (c) pre-existing non-equilibrium vacancy concentrations in the deposited multilayer.

Mathematical description of planar single phase growth (even in non-isothermal conditions) is easier than that of interdiffusion with variable diffusivity. So, in this communication we will present:

- basic model with iteration procedure for finding the steady-state characteristics of planar SHS front (Section 2);
- analytical approximation to calculating the front propagation velocity (Section 3);
- scaling analysis of the obtained dependences (Section 4);
- modified algorithm with account of vacancy subsystem inertia with respect to temperature evolution (Section 5.1);
- modified algorithm with account of initial vacancy supersaturation in asprepared foils (Section 5.2).

2. BASIC MODEL

Let us consider a binary multilayered foil of width W initially consisting of M alternating nanolayers of compounds A and B taken in a 1 : 1 stoichiometric ratio (Fig. 1), each of thickness $2l$, so that the multilayer period is $4l$. For simplicity, we will assume the atomic volumes to be equal for both the components and resultant product. Starting components are consumed simultaneously, without surplus. At each interface, there exists a thin layer of product phase with thickness Δy_0.

In contrast to [8], we will assume that heat release is localized only at the moving interphase boundaries. At that, we will use the equation of reactive diffusion that is applicable to compounds with a narrow homogeneity range.

Basic model assumptions are enumerated below.

(1) The reaction front is considered as steadily propagating along axis x at constant burning velocity V.

(2) Front width L is much wider than multilayer period $4l$.

(3) All diffusion fluxes are directed normally to temperature gradient.

(4) Temperature variation along the direction of diffusion flux (axis y) is neglected.

(5) The former three assumptions are valid when $a^2L/V \gg l^2$ (a is thermal diffusivity).

(6) The intermediate stoichiometric phase AB (δ-phase) with the narrow homogeneity range $c_{\text{left}} < c < c_{\text{right}}$ ($\Delta c \equiv c_{\text{right}} - c_{\text{left}} \ll 1$) is the first phase to grow and simultaneously the end product.

(7) All concentrations at all interphase boundaries are regarded as quasi-equilibrium ones: composition at both sides of each boundary corresponds to the common tangent rule for local temperature.

(8) Diffusion through a newly formed product layer is treated as a quasi-steady process, due to almost constant concentration in the compound phase. In this case, the approximation of constant flux is applicable [9]. It means that the flux densities J_{left}, J_{right} at the left and right boundaries are practically equal to each other and to the flux density inside the phase layer. This flux is determined in terms of averaged value $\overline{D}$ of the interdiffusivity concentration dependence $D(c)$:

$$J_{\text{left}} \sim J_{\text{right}} \sim J = -\frac{\frac{1}{\Omega}\int_{c_{\text{left}}}^{c_{\text{right}}} D(c)dc}{x_{\text{right}} - x_{\text{left}}} = -\frac{\frac{1}{\Omega}\overline{D}\Delta c}{x_{\text{right}} - x_{\text{left}}},$$

where Ω is the atomic volume.

(9) All diffusivities are proportional to vacancy concentration which is considered, so far, as a quasi-equilibrium one corresponding to actual local temperature.

(10) The heat is released only at the moving interphase boundary but almost instantly and uniformly and is distributed within each thin slice transversal to front propagation direction.

(11) Heat outflux via side walls of multifoil is neglected.

Mann et al. [8] treated the self-consistent mathematical problem of simultaneous non-isothermal interdiffusion and temperature redistribution. Namely, the solution of second Fick's law gave the time evolution of

concentration profiles, which was recalculated into the heat release over the entire diffusion zone. Heat release changes temperature, changing temperature changes diffusivity, changing diffusivity changes intermixing rate, changing intermixing rate changes the heat release—and this is an SHS cycle. In this paper, we limit ourselves to compound growth that can be described much easier. During such a growth, the heat release proceeds only at the moving interphase boundaries. Moreover, in this case one can make easier account of non-equilibrium factors (see Section 5).

Let us consider the diffusion-controlled growth of δ-phase between the α-phase (diluted solution of B in A) and ζ-phase (diluted solution of A in B) with the driving force $\Delta g_{\delta(\alpha,\zeta)}$ (Fig. 2) [10]. The driving force of reaction depends on temperature but this dependence is much weaker than the Arrhenius temperature dependence of diffusivity. Thus we assume $\Delta g_{\delta(\alpha,\zeta)}$ to be constant.

Sample representing morphology of whole system (Fig. 3) has thickness $2l$ (half a multilayer period).

In the thin slice dx perpendicular to the direction of front propagation (Fig. 4), increment in new phase thickness $d\Delta y_\delta(x)$ will proceed during time $dt = dx/V$. In reactive diffusion, heat is released only at the moving boundaries at both sides of the growing phase (Fig. 4). This heat is equal $\Delta g_{\delta(\alpha,\zeta)} d\Delta y_\delta(x) \times dx \times W/\Omega$. According to model assumption 10, it is uniformly distributed over the slice volume $2l \times dx \times W$. Thus, the heat release rate per unit volume (local heat source) is given by:

$$q_\delta(x) = \frac{\Delta g_{\delta(\alpha,\zeta)} d\Delta y_\delta(x) \times dx \times W/\Omega/dt}{2l \times dx \times W} = \frac{\Delta g_{\delta(\alpha,\zeta)} d\Delta y_\delta(x)}{2l\Omega dt}, \quad (1)$$

In our case, SHS modeling means simultaneous solution of phase growth kinetic equation (with diffusivity dependent on temperature which is, in its turn, dependent on time) and temperature redistribution equation [with heat source $q_\delta(x)$ proportional to the local growth rate]. Mathematically, the model gives self-consistent profiles of temperature $T(x)$ and phase width $\Delta y(x)$ by simultaneous solution of equations for single phase growth in non-isothermal conditions and for temperature evolution under heat release.

The kinetic equations for phase growth can be written as:

$$\begin{cases} (c_\delta - 0)\dfrac{\partial y_{\alpha\delta}(t,x)}{\partial t} = -\dfrac{D_\delta T(t,x)\Delta c_\delta}{y_{\delta\zeta} - y_{\alpha\delta}} \\ (1 - c_\delta)\dfrac{\partial y_{\delta\zeta}(t,x)}{\partial t} = +\dfrac{D_\delta T(t,x)\Delta c_\delta}{y_{\delta\zeta} - y_{\alpha\delta}}, \end{cases} \quad (2)$$

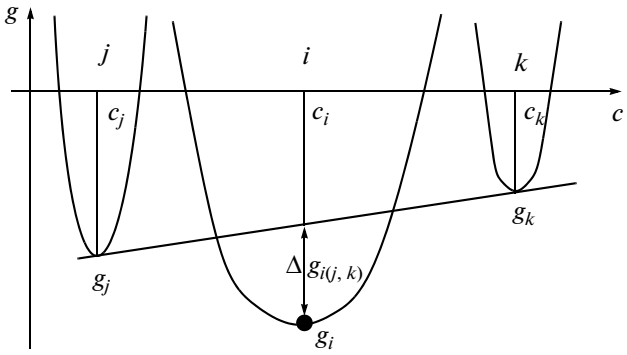

Fig. 2. Thermodynamic driving force $\Delta g_{i(j,k)}$, the Gibbs free energy per atom released during formation of the i-phase from phases j and k under constraint mass balance: $\Delta g_{i(j,k)} = c_k - c_i/c_k - c_j g_j + c_i - c_j/c_k - c_j g_k - g_i$.

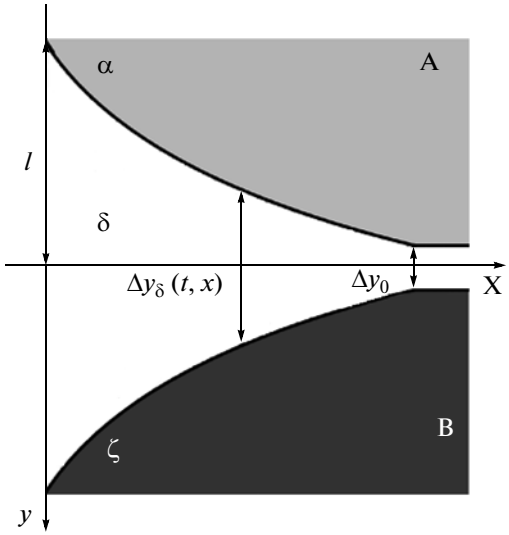

Fig. 3. Geometry adopted in the model for δ-phase growth.

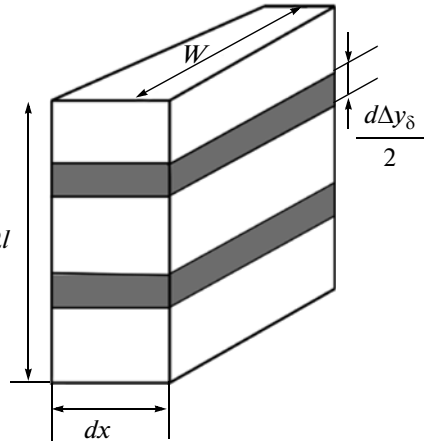

Fig. 4. Layer $d\Delta y_\delta$ from which heat release takes place during time period dt.

where c_δ is the average concentration, D_δ average interdiffusivity, and Δc_δ homogeneity range of the δ-phase.

Equation (2) can be easily reduced to the form:

$$\frac{d\Delta y_\delta^2(t,x)}{dt} = \frac{2}{c_\delta(1-c_\delta)} D_\delta T(t,x)\Delta c_\delta, \qquad (3)$$

where $\Delta y_\delta(t,x) = y_{\delta\zeta} - y_{\alpha\delta}$.

One can markedly simplify Eqs. (2), (3) using (a) the concept of Wagner diffusivity and (b) steady-state treatment. Of course, steady-state solutions should be checked for their stability and uniqueness.

Direct experimental measurement of homogeneity range Δc_δ is often impossible but the phase growth kinetics is determined by the magnitude $D_\delta^W = D_\delta \Delta c_\delta$ called Wagner diffusivity [9, 11]. It can be easily shown that the Wagner diffusivity can be expressed in terms of tracer diffusivities D_A^*, D_B^* inside the phase and driving force of transformation $\Delta g_{\delta(\alpha,\zeta)}(T)$:

$$D_\delta^T T(t,x) = (c_\delta D_A^* + (1-c_\delta) D_B^*) \times \Delta g_{\delta(\alpha,\zeta)} T(t,x)/k_B T(t,x), \qquad (4)$$

Its temperature dependence obeys the "nearly Arrhenius" law:

$$D_\delta^W = D_{\delta 0}^W \exp(-Q_\delta/kT)\Delta g_{\delta(\alpha,\zeta)}/k_B T. \qquad (5)$$

So far, we confine ourselves to steady-state solution of set (2), (3). In this case, we can reduce the number of variables from two to one:

$$\tilde{x} = x - Vt, \begin{cases} \tilde{x} < 0 & \text{beyond front} \\ 0 < \tilde{x} & \text{at front.} \end{cases}$$

At $\tilde{x} = 0$, the layers merge: $\Delta y_\delta(t, 0) = 2l$ (Fig. 3). Equation (3) has the following formal solution (it is necessary to take into account that layer $\Delta y_\delta(t, x)$ contains a premixed layer thickness Δy_0 with diffusivity $D_{\delta 0}^W$ in which the reaction already passed):

$$\Delta y_\delta^2(\tilde{x}) = \Delta y_0^2 + \frac{2}{c_\delta(1-c_\delta)} \frac{1}{V} \int_{\tilde{x}}^{+\infty} (D_\delta^W T(\xi) - D_{\delta 0}^W) d\xi. \qquad (6)$$

Combining Eq. (6) with convergence conditions, we obtain the expression for front propagation velocity V:

$$V = \frac{1}{4l^2 - y_{0\delta}^2} \frac{2}{c(1-c_\delta)} \int_0^{+\infty} (D_\delta^W T(\xi) - D_{\delta 0}^W) d\xi. \qquad (7)$$

Now let us consider the heat conductivity equation $\partial T/\partial t = a^2\, \partial T/\partial x + q_\delta(t, x)/c_p\rho$ with the heat source defined by Eq. (1), preliminary replacing $dt = d\tilde{x}/V$ (here c_p is the specific heat capacity and ρ density):

$$-V\frac{\partial T}{\partial \tilde{x}} - a^2 \frac{\partial^2 T}{\partial \tilde{x}^2} = \begin{cases} 0, & \tilde{x} < 0, \Delta y(\tilde{x}) - 2l \text{ beyond the front} \\ q_\delta(\tilde{x})/c_p\rho, & 0 < \tilde{x}, \ \Delta y_0 < \Delta y(\tilde{x}) < 2l \text{ at the front.} \end{cases} \qquad (8)$$

A formal steady-state solution to Eq. (8) is the following integral equation:

$$T(\tilde{x}) = \begin{cases} T_0 + \dfrac{1}{V}\displaystyle\int_0^\infty \frac{q_{\delta(\alpha,\zeta)} T(\xi)}{c_p\rho} d\xi, & \tilde{x} < 0 \\ T_0 + \dfrac{1}{V}\displaystyle\int_{\tilde{x}}^\infty \frac{q_{\delta(\alpha,\zeta)} T(\xi)}{c_p\rho} d\xi, + \dfrac{1}{V}\displaystyle\int_0^{\tilde{x}} \frac{q_{\delta(\alpha,\zeta)} T(\xi)}{c_p\rho} \exp\left(\frac{V}{a^2}(\xi - \tilde{x})\right) d\xi, & 0 < \tilde{x}. \end{cases} \qquad (9)$$

This equation can be solved together with Eq. (7) by applying a self-consistent iteration procedure for simultaneous determination of temperature profile and burning velocity.

3. ANALYTICAL APPROXIMATION

We attempted to simplify the above model and to avoid the iteration procedure. Namely, we suggest the following analytical approximation. Let us assume for a while that we may ignore the heat source in Eq. (8), $-V\,\partial T/\partial x - a^2 \partial^2 T/\partial x^2 = 0$, and thus obtain the solution:

$$\frac{\partial T}{\partial x} = \left(\frac{\partial T}{\partial x}\right)_0 \exp\left(-\frac{V}{a^2}x\right) \sim \exp\left(-\frac{x}{L}\right), \qquad (10)$$

where $L = a^2/V$ is the front width.

As a result of reactive diffusion during time $\tau \sim L/V = a^2/V^2$, the front pathways at width L of the δ-phase (equilibrium concentration c_δ) can converge:

$$\frac{2}{c_\delta(1-c_\delta)} \int_0^\tau D_\delta^W T(t) dt \approx (2l)^2 - (\Delta y_0)^2. \qquad (11)$$

Integration of (11) with the use of simple but bulky algebra will lead to the following approximate expression for flame propagation velocity V:

$$V = \sqrt{\frac{2}{c_\delta(1-c_\delta)}\frac{a^2 D^W_{\delta 0}\Delta g_{\delta(\alpha,\zeta)}}{4l^2-\Delta y_0^2}\frac{T_0(k_B T_f+Q)}{Q_\delta^2(T_f-T_0)}\exp\left(-\frac{Q_\delta}{k_B T_f}\right)}, \quad (12)$$

where T_f is the maximal front temperature. Certainly, due to neglecting the heat source in analytical approximation for temperature profile, one should be ready for further modification of expression (12) by introducing some fitting factors.

For estimation of T_f we used formula (1). Since a maximal temperature is achieved through time τ of reaction in the effective layer thickness $2l - \Delta y_0$, this temperature change is given by

$$T_f - T_0 = \int_0^\tau \frac{q_\delta(x)}{c_p\rho}dt' = \frac{\Delta g_{\delta(\alpha,\zeta)}(2l-\Delta y_0)}{2lc_p\rho\Omega}. \quad (13)$$

Obviously, the larger is the initial layer thickness Δy_0, the lower will be a maximal front temperature T_f. A maximal value of T_f, $T_0 + \Delta g_{\delta(\alpha,\zeta)}/c_p\rho\Omega$, is attained at $\Delta y_0 = 0$.

To quantify the influence of preexisting layer, we introduced the parameter $f = (2l - \Delta y_0)/2l$ that defines a fraction of unreacted components in bilayer $2l$. Since f characterizes the efficiency of SHS reaction (the front temperature achieves a maximum at $f \cong 1$), it can be termed as "multilayer efficiency".

Multilayer efficiency can vary from zero (pure components are absent and SHS reaction is impossible) to unity (SHS reaction takes place over the entire foil). In computer-assisted calculations the f values were taken from the range $0.5 \le f < 1$, because multilayer foils with $f < 0.5$ seem to be ineffective for SHS.

In the following sections, we will compare the results of numerical iterative method with our analytical approximation. We will show that not only qualitative but also quantitative coincidence can be reached by using only one fitting parameter in analytical expressions (10), (12):

$$L = p\frac{a^2}{V}, \quad (10^*)$$

$$V = \sqrt{p\frac{2}{c_\delta(1-c_\delta)}\frac{a^2 D^W_{\delta 0}\Delta g_{\delta(\alpha,\zeta)}}{4l^2-\Delta y_0^2}\frac{T_0(k_B T_{\delta f}+Q)}{Q_\delta^2(T_f-T_0)}\exp\left(-\frac{Q_\delta}{k_B T_f}\right)}, \quad (12^*)$$

where

$$T_f = T_0 + (T_{max} - T_0)f. \quad (13^*)$$

4. SCALING ANALYSIS

As follows from semi-analytical relationship (13*), the product lV must be a function of only multilayer efficiency f and to remain unchanged upon variation in l at constant f. Indeed, representing the term $1/4l^2 - \Delta y_0^2$ in Eq. (13*) as $1/4l^2 f(2-f)$ and multiplying both parts of Eq. (13*) by l, we obtain:

$$lV(l,f) = \sqrt{\text{const}\frac{1}{f(2-f)}\frac{(k_B T_{\delta f}(f)+Q)}{(T_f(f)-T_0)}\exp\left(-\frac{Q_\delta}{k_B T_f(f)}\right)} = \text{function}(f). \quad (14)$$

Scaling in Eq. (14) indicates a possibility of optimizing the fit of SHS parameters. As multilayered foils are non-equilibrium objects, it is impossible to guarantee that the diffusivity and thermodynamics parameters of our model can be taken from tables of physical constants. First of all, it concerns the activation energy for diffusion Q_δ and pre-exponential factor $D^W_{\delta 0}\Delta g_{\delta(\alpha,\zeta)}$ in the Wagner diffusivity. We suggest to interpret them as adjustment parameters in Eq. (12*). Note that the derivative of $\ln(lV)$ with respect to f (with account of Eq. (14)) relies on the only parameter Q_δ:

$$\frac{d\ln(lV)}{df} = \frac{1}{2}\ln\left(\frac{1}{f^2(2-f)}\frac{Q_\delta}{(T_{max}-T_0)}\right) - \frac{Q_\delta}{k_B T_f(f)}.$$

Comparison with an experimental curve affords to fit the parameter Q_δ. The fitted value of Q_δ can be used for finding the second free parameter, $D^W_{\delta 0}\Delta g_{\delta(\alpha,\zeta)}$.

5. ROLE OF FINITE VACANCY RELAXATION RATE

The aim of this section is to check it out whether or not the account of non-equilibrium vacancy concentration is vital for predicting the SHS kinetics.

We will take into account the non-equilibrium concentration of vacancies during SHS by considering the following two competing non-equilibrium processes.

(1) When the temperature locally rises, the equilibrium concentration also rapidly rises. However, the

Maximum (over varying multilayer period) front velocities V (in m/s) at different values of L_v and c_v^{noneq}

c_v^{noneq}	L_v, nm		
	0	5	160
10^{-4}	220.92	66.71	66.47
5×10^{-5}		47.30	47.00
10^{-5}		31.96	21.06
0		29.91	5.42

actual vacancy concentration will be much lower since vacancies need some time for their generation and distribution over the bulk. Local reaction rate is determined by the local diffusivity which in turn is proportional to local vacancy concentration. Thus, a finite rate of vacancy relaxation must slow down heat release and hence the SHS reaction.

(2) On the other hand, as-prepared multilayer may contain extra vacancies from the very beginning. Concentration of these initial extra vacancies depends on (a) the deposition rate, (b) substrate temperature during foil preparation, (c) waiting time, and (d) initial temperature. Initial extra vacancies can be expected to accelerate the reaction. Moreover, initial non-equilibrium state must lead to higher energy release from the reaction.

Below, we will explore the effect of both abovementioned factors.

First, let us reformulate the steady-state problem for SHS in multifoil (yielding single-phase product) under the assumption of vacancy quasi-equilibrium. Our algorithm and iterative numeric scheme differ from earlier ones [8] but give essentially the same results at the same set of model parameters.

Second, we will modify the suggested model by taking into account finite rates of vacancy generation and annihilation. Unfortunately, in this case only a numerical scheme can be realized. We will explore the influence of the vacancy sources efficiency on the parameters of SHS reaction.

Third, we will incorporate the initial extra vacancies as an initial condition into our scheme and trace the influence of initial supersaturation on SHS characteristics.

5.1. Role of Vacancy Subsystem Inertia

We will calculate the rate of the reaction controlled by reactive diffusion. The reaction rate is determined by diffusivity within the newly formed product layers. Diffusivity of atoms is controlled by vacancy mechanism and proportional to actual vacancy concentration. Instead, so far we used the diffusivity calculated via Arrhenius law with activation energy equal to the sum of vacancy formation enthalpy H_V^{form} and vacancy migration enthalpy H_V^{migr}. It means that the used diffusivities were proportional to quasi-equilibrium vacancy concentration:

$$c_V^{eq} T(t,x) = \exp\left(-\frac{H_V^{form}}{kT(t,x)}\right). \quad (15)$$

The same implicit assumption was used in previous models [8, 12]. Instead, to be more close to reality, one should take into account the inertial properties of vacancy concentration related to the finite relaxation time τ_v of vacancies. Indeed, the time of temperature rise from room temperature to one–two thousands degrees in the flame front (L/V) is typically less than a microsecond. During this time, the extra vacancies needed by higher temperature for local quasi-equilibrium, have not enough time to be generated and distributed over the system to provide quasi-equilibrium diffusivity of atoms. So, we must replace the Wagner diffusivity $D_\delta^W T(\tilde{x})$ by

$$D(\tilde{x}) = \frac{c_v(\tilde{x})}{c_v^{eq} T(\tilde{x})} D_\delta^W T(\tilde{x}). \quad (16)$$

Here the actual local vacancy concentration is determined by the relaxation equation:

$$\frac{\partial c_v(t,x)}{\partial t} = -\frac{1}{\tau_v}(c_v - c_v^{eq})$$
$$= -\frac{D_{v0}\exp\left(-\frac{H_V^{migr}}{kT(t,x)}\right)}{L_v^2}(c_v(t,x) - c_v^{eq} T(t,x)). \quad (17)$$

Here the mean free pathlength of vacancies L_v is treated as a constant. (Actually, it may change due to evolution of interphase boundaries.) In case of steady-state solution (so that $\partial/\partial t = -V\partial/\partial\tilde{x}$), it transforms into

$$\frac{dc_v(\tilde{x})}{d\tilde{x}} = +\frac{D_{v0}\exp\left(-\frac{H_v^{migr}}{kT(\tilde{x})}\right)}{VL_v^2}(c_v(\tilde{x}) - c_v^{eq} T(\tilde{x})), \quad (18)$$
$$c_v(\tilde{x} \to \infty) = c_v^{pre-exist} = c_v(T^{room}).$$

Thus, one has (at each iteration step) to solve Eq. (18), substitute the result into Eq. (15), and the result of this substitution, into Eq. (7) of the self-consistent numerical iteration scheme.

5.2. Role of Pre-Existing Vacancy Supersaturation in As-Prepared Multilayers

Since the formation of initial multilayer is a non-equilibrium process, the pre-existing multilayered foil, typically, is a non-equilibrium structure whose fea-

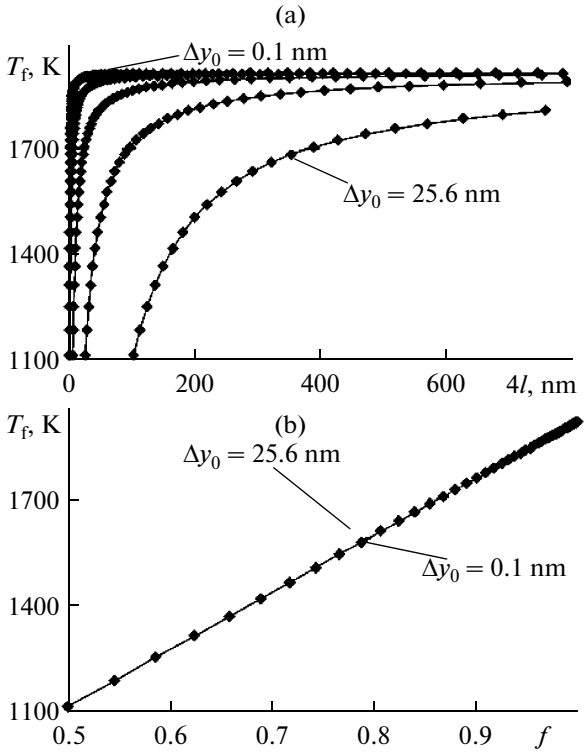

Fig. 5. Maximal front temperature T_f as a function of multilayer period $4l$ (a) and multilayer efficiency f (b) at various values of initial (pre-existing) phase thickness Δy_0 (= 0.1, 0.4, 1.6, 6.4, and 25.64 nm): calculations by numerical model (data points) and by Eq. (13*) of semi-analytical model (solid lines).

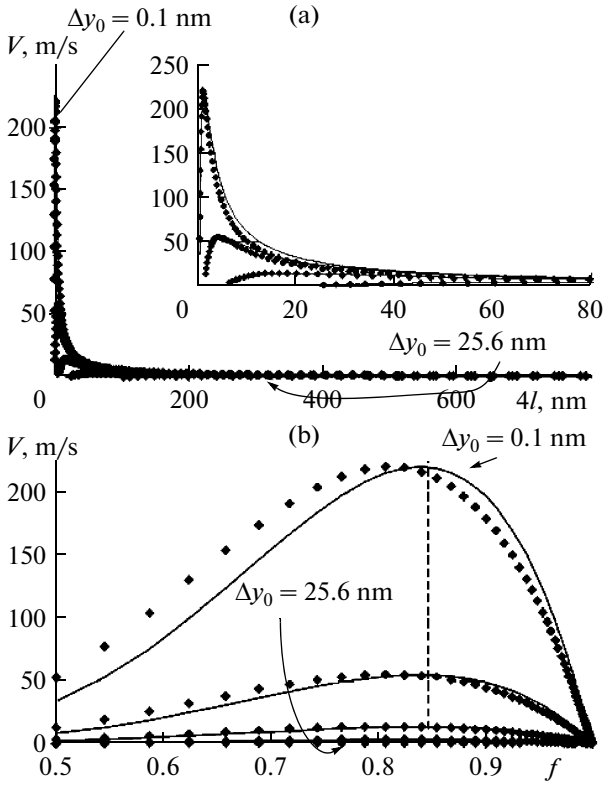

Fig. 6. Front velocity V as a function of multilayer period $4l$ (a) and multilayer efficiency f (b) at various values of initial (pre-existing) phase thickness Δy_0: calculations by numerical model (data points) and by Eq. (12*) of semi-analytical model (solid lines) at $p = 4.04$. Note that maximal values of all velocity profiles in (b) (velocity as a function of f at fixed Δy_0) are different but all of them correspond to the same value 0.85 (dotted line) of multilayer efficiency f.

tures are defined by the values of deposition flux and substrate temperature. Here we will confine ourselves to considering a non-equilibrium state related to pre-existing ("frozen in") isolated vacancies with additional concentration c_v^{noneq}. Thus, we have to change the initial conditions for the differential equation

$$c_v(\tilde{x} \to \infty) = c_v^{\text{pre-exist}} = c_v(T^{\text{room}}) + c_v^{\text{noneq}}. \quad (19)$$

After this, the above-described iteration procedure is applied to obtain temperature profiles and propagation velocity.

6. RESULTS AND DISCUSSION

First of all, we compared the results of numerical iteration under the assumption of quasi-equilibrium vacancy concentration with predictions of analytical expressions (12) and (13). Set of equations (6), (7), (9) was solved by iteration procedure providing self-consistent temperature profile and propagation velocity. The following parameters were used: $c_\delta = 0.5$, $D^*_{0\delta} = 1.5 \times 10^{-5}$ m^2/s, $Q = 2.7 \times 10^{-19}$ J, $a^2 = 7.42 \times 10^{-5}$ m^2/s, $T_0 = 300$ K, $T_f = 1919$ K [8]. The thermodynamic driving force for the growth of δ-phase, $\Delta g_{\delta(\alpha,\,\zeta)} = 7.37 \times 10^{-20}$ J, was calculated from estimation (13) for maximal temperature at $\Delta y_0 = 0$ and $T_f = 1919$ K.

A value of l (fourth of multilayer period) was varied from y_0 ($f = 0.5$, half a premixed layer) to 200 nm (maximal period of multilayer $4l$ did not exceed 800 nm). The thickness of premixed layer Δy_0 was changed from 0.1 nm (less than an interatomic distance corresponding to $f \cong 1$) to the l value corresponding to $f = 0.5$.

During computer calculations at premixed layer thickness Δy_0 or/and various multilayer thickness $4l$, the following characteristics were determined: (a) maximal front temperature T_f (Fig. 5a, data points) and (b) front velocity V from Eq. (7) (Fig. 6a, data points). The results were compared with estimations of the simplified analytical model for the front velocity (12) at the maximal temperature (13). Results for numeric iterative procedure and for simplified analytical model qualitatively coincided. After multiplying by the fitting parameter $p = 4.04$ in Eq. (12*), this coincidence became quantitative as is seen in Fig. 6a (solid lines). So far we cannot explain why the fitting parameter is so close to 4. Corresponding dependences of maximal temperature and front velocity on multilayer

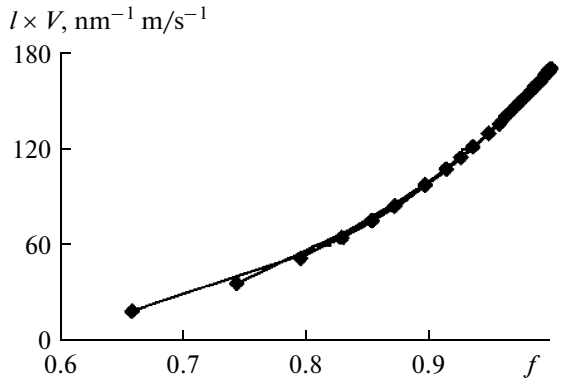

Fig. 7. Product lV vs. multilayer efficiency f at fixed l (= 50, 75, 100, 125, 150, and 175 nm): change in f is caused by a change in premixed layer thickness Δy_0. For large f, all six dependencies are seen to be practically coincident.

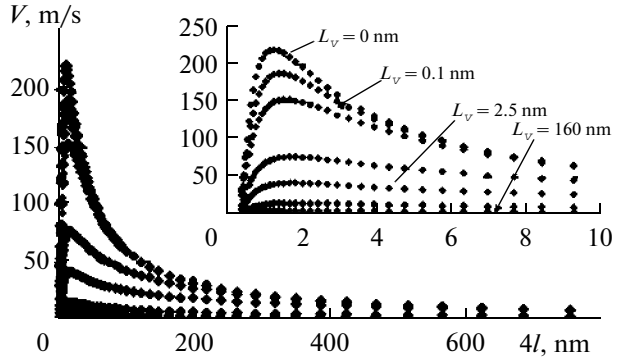

Fig. 8. Front velocity V vs. multilayer period $4l$ at fixed $\Delta y_0 = 0.1$ nm for various values of L_v. The curve for $L_v =$ 0 nm was calculated with no account for any deviation from equilibrium vacancy concentration and corresponds to one of the curves in Fig. 5a.

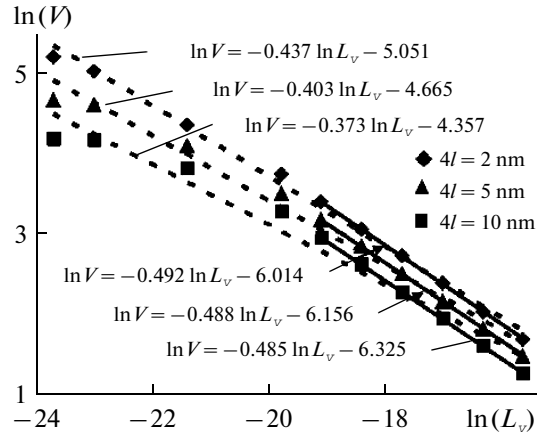

Fig. 9. Front velocity V vs. mean vacancy free pathlength L_v (in logarithmic scale) for various values of $4l$ at pre-existing phase thickness $\Delta y_0 = 0.1$ nm for "large" L_v (solid lines) and for a full range of L_v (dashed lines).

period and "multilayer efficiency" $f = (2l - \Delta y_0)/(2l)$ are given in Figs. 5b, 6b.

The dependence of temperature on the multilayer period $4l$ and on premixed layer thickness Δy_0 is determined by the multilayer efficiency f and fits a linear law (Fig. 5b). At fixed Δy_0, the asymptotic magnitude of maximal temperature in the flame is reached when the "parasitic" premixed layer can be neglected; in other words, when the multilayer period is significantly larger than the premixed layer. Therefore, the thicker is the premixed layer, the larger is the $4l$ value providing asymptotic temperature magnitude (Fig. 5a). A decrease in front velocity V with decreasing f (below 0.5) can be easily explained. Qualitatively, small f values mean that the majority of atoms have reacted ahead of the reaction front. This factor sharply suppresses local heating and, hence, the front velocity. On the other hand, large f values mean that initial layers are thick and hence reaction times are longer, which also leads to a decrease in V. Thus, a maximal velocity V can be expected for some intermediate f values. As we have just seen, this intermediate value in our case was about 0.85, but it depends on the activation energy of reactive diffusion. Indeed, a change in activation energy from $Q = 2.7 \times 10^{-19}$ J to $Q = 1.35 \times 10^{-19}$ J leads to the optimal value $f = 0.675$.

Non-monotonous dependences of front velocity V on multilayer period $4l$ (Fig. 6a) are similar to those numerically modeled by Mann et al. [8] and consistent with reported experimental data for the Ti–Al system [13].

To check the scaling predicted by semi-analytical approximation (14) and by rigorous numerical scheme, we plotted lV as a function of f at varied Δy_0 and fixed l. As is seen in Fig. 7, the curves turned out practically coincident.

To study the influence of finite vacancy relaxation rate, we changed the expression for diffusivity using Eq. (16). The actual local vacancy concentration used in Eq. (16) was calculated according to Eq. (18). Then we used the above-mentioned iteration scheme. We investigated the dependences of V on $4l$ for various vacancy mean free pathlengths L_v. As follows from Fig. 8, the calculated velocities V decrease substantially after the finite relaxation time has been taken into account. In this figure we demonstrate one set of plots at fixed Δy_0, other Δy_0 dependences being similar but shifted.

We have found that, for $L_v > 0.5$ nm, the dependence of V on $1/L_v$ is well fitted by the nearly parabolic function:

$$V(L_v, \delta) \approx k(\delta)/\sqrt{L_v}. \qquad (20)$$

For very small values of L_v (formally tending to zero), this dependence just cannot be valid, since the front velocity is finite even at ideal work of vacancy sources (zero relaxation time). To illustrate this peculiarity, Fig. 9 presents the fitting $V(L_v)$ of dependence in logarithmic scale for "large" L_v with an almost ideal

power close to −0.5 (solid lines) and for a full range of L_v with substantially less power (dashed lines). Moreover, the less is $4l$, the closer is power to a value of −0.5. The coefficient $k(\delta)$ in Eq. (20) depends on multilayer period similarly to $V(\delta)$.

Account of pre-existing vacancies ("frozen-in" during multifoil preparation) was made according to Eq. (19). We present only some particular cases (table) to check out whether or not the role of pre-existing vacancies is important.

The larger is L_v (larger relaxation time), the more vivid is the influence of initial supersaturation on V: at $L_v = 5$ nm, the velocity changes by a factor of two while at $L_v = 160$ nm, by more than an order of magnitude. If L_v tends to zero, initial supersaturation loses its influence, since in this case the vacancy subsystem immediately adapts to changing temperature. The influence of initial deviation from equilibrium on SHS in powder mixtures has been recently analyzed in [14]. So far we did not manage to find an "analytical" interpretation of rather vivid power law in Eq. (20). In any case, it cannot be a general law since, at $L_v \to 0$, Eq. (20) unrealistically gives infinity for the propagation velocity. Yet, for not very small L_v fitting (20) works fairly well.

Of course, the finite vacancy relaxation rate is not a unique reason for reaction retardation. Finite time of intermetallic phase nucleation and lattice reconstruction may also be important. Yet, from isothermal reactive diffusion we know that, at least for high temperatures, the finite diffusion rate is a controlling factor of reaction. Finite rate of lattice reconstruction will be discussed elsewhere.

One more possible reason for slowing down the SHS rate is an initial oxidation of multilayer thin films during deposition. It may lead to formation of thin barrier oxide films at the interfaces. Formally, in this case one should change Eq. (3) by adding some characteristic length λ to $\Delta y_\delta(t, x)$ in the denominator of the right-hand side of Eq. (3). This characteristic length should be proportional to diffusivity and inversely proportional to the effective interface rate coefficient [15].

CONCLUSIONS

(1) Phenomenological model of SHS diffusion-controlled reaction in multifoils yielding a single reaction product with heat source at the moving interface boundaries gives, qualitatively, the same results as model [8] with distributed heat sources in the diffusion zone. Our model is steady-state and based on iterative solution of the equations of reactive diffusion and heat conduction.

(2) Crude analytical approximation (12), (13) fairly well describes the same process after introducing only one fitting parameter.

(3) SHS, at least in a steady-state regime, demonstrates a scaling behavior: the product of front velocity and of multilayer period depends only on one parameter, multilayer efficiency. This scaling, in principle, can be used for fitting diffusion parameters in strongly non-equilibrium systems.

(4) The finite rate of vacancy relaxation leads to a substantial decrease (almost inversely proportional to vacancy mean free path) in the front propagation velocity and to broadening the flame front.

(5) Conversely, pre-existing vacancies (frozen-in after fast deposition on the cold substrate) increase the front velocity. The effect is not so pronounced as the influence of the finite relaxation rate, but it becomes perceptible if the mean free pathlength of vacancies is long.

ACKNOWLEDGMENTS

This work was supported by the Ministry for Education and Science, Ukrainian Foundation for Basic Research, and National Academy of Sciences (program *Fundamental problems of nanostructured systems, nanomaterials, and nanotechnologies*).

REFERENCES

1. Merzhanov, A.G., On Critical Conditions for Thermal Explosion in a Hot Spot, *Combust. Flame*, 1966, vol. 10, no. 4, pp. 341–348.
2. Ma, E., Thompson, C.V., Clevenger, L.A., and Tu, K.N., Self-Propagating Explosive Reactions in Al/Ni Thin Films, *Appl. Phys. Lett.*, 1990, vol. 57, no. 12, pp. 1262–1264.
3. Clevenger, L.A., Thompson, C.V., and Tu, K.N., Explosive Silicidation in Nickel/Amorphous Silicon Multilayer Thin Films, *J. Appl. Phys.*, 1990, vol. 67, no. 6, pp. 2894–2898.
4. Gennari, S., Tamburini, U.A., Maglia, F., Spinolo, G., and Munir, Z.A., A New Approach to the Modeling of SHS Reactions: Combustion Synthesis of Transition Metal Aluminides, *Acta Mater.*, 2006, vol. 54, no. 9, pp. 2343–2351.
5. Merzhanov, A.G. and Mukasyan, A.S., *Tverdoplamennoe gorenie* (Solid-Flame Combustion), Moscow: Torus Press, 2007.
6. Ishchenko, A.Ya., Falchenko, Yu.V., Ustinov, A.I., Movchan, B.A., Kharchenko, G.K., Muraveinik, A.N., Melnichenko, T.V., and Rudenko, A.E., Diffusion Welding of Finely Dispersed AMg5/27% Al_2O_3 Composite with Application of Nanolayered Ni/Al Foil, *Paton Welding J.* (Kiev), 2007, no. 7, pp. 2–5.
7. Ustinov, A.I., Falchenko, Yu.V., Ischenko, A.Ya., Kharchenko, G.K., Melnichenko, T.V., and Muraveinik, A.N., Diffusion Welding of γ-TiAl Based Alloys through Nano-Layered Foil of Ti/Al System, *Intermetallics*, 2008, vol. 16, no. 8, pp. 1043–1045.
8. Mann, B., Gavens, A.J., Reiss, M.E., Van Heerden, D., Bao, G., and Weihs, T.P., Modeling and Characterizing the Propagation Velocity of Exothermic Reactions in Multilayer Foils, *J. Appl. Phys.*, 1997, vol. 82, no. 3, pp. 1178–1188.
9. Gusak, A.M. and Yarmolenko, M.V., A simple Way of Describing the Diffusion Phase Growth in Cylindrical

and Spherical Samples, *J. Appl. Phys.*, 1993, vol. 73, no. 10, pp. 4881–4884.

10. Gusak, A.M., Zaporozhets, T.V., Kornienko, S.V., Lyashenko, Y.A., Pasichny, M.O., and Shirinyan, A.S., *Diffusion-Controlled Solid State Reactions in Alloys, Thin Films, and Nanosystems*, Berlin: Wiley–VCH, 2010.
11. Wagner, C., The Evaluation of Data Obtained with Diffusion Couples of Binary Single-Phase and Multiphase Systems, *Acta Metall.*, 1969, vol. 17, no. 2, pp. 99–107.
12. Zaporozhets, T.V., Gusak, A.M., and Ustinov, A.I., Modeling of SHS-Reaction Steady -State Regime in Nanofoils (Phenomenological Model), Vol. 1: Single-Stage Reaction, *Adv. Electrometall.*, 2010, no. 1, pp. 40–46.
13. Rogachev, A.S., Grigoryan, A.E., Illarionov, E.V., Kanel, I.G., Merzhanov, A.G., Nosyrev, A.N., Sachkova, N.V., Khvesyuk, V.I., and Tsygankov, P.A., Gas-Free Combustion of Multilayered Bimetallic Nanofoils Ti/Al, *Fiz. Goreniya Vzryva*, 2004, vol. 40, no. 2, pp. 45–51.
14. Khina, B.B., Effect of Mechanical Activation on SHS: Physicochemical Mechanism, *Int. J. SHS,* 2008, vol. 17, no. 4, pp. 211–217.
15. Goesele, U. and Tu, K.N., Growth Kinetics of Planar Binary Diffusion Couples: "Thin-Film Case" versus "Bulk Cases", *J. Appl. Phys.*, 1982, vol. 53, no. 4, pp. 3252–3260.